Numerical Modeling on the Stress-Strain Response and Fracture of Modeled Recycled Aggregate Concrete

Wengui Li[1,2], Jianzhuang Xiao[1,*], David J. Corr[2], Surendra P. Shah[2]

[1] Department of Building Engineering, Tongji University, Shanghai 200092, China
[2] Center for Advanced Cement-Based Materials, Northwestern University, Evanston 60208, USA
* Corresponding author: jzx@tongji.edu.cn

Abstract According to the nanoindentation tests, the constitutive relationship of the Interfacial Transition Zones (ITZs) in Recycled Aggregate Concrete (RAC) is proposed with a plastic-damage constitutive model. Based on the meso/micro-scale constitutive relations of mortar matrix, numerical studies were undertaken on Modeled Recycled Aggregate Concrete (MRAC) under uniaxial loadings to predict mechanical behavior, particularly the stress-strain response. The tensile stress tends to concentrate in the ITZs region, which leads to the development of microcracks. After the calibration and validation with experimental results, the effects of the mechanical properties of ITZs and new mortar matrix on the stress-strain response and fracture of MRAC were analyzed. The FEM modeling is capable of simulating the complete stress-strain relationship of MRAC, as well as the overall fracture pattern. It reveals that the mechanical properties of new mortar matrix and the corresponding new ITZ play a significant role in the overall stress-strain response and fracture process of MRAC.

Keywords Modeled recycled aggregate concrete (MRAC), Interfacial transition zones (ITZs), Plastic-damage constitutive model, Stress-strain response, Fracture

1. Introduction

Most of cement-based materials have intrinsic heterogeneous and nonlinear mechanical behaviors due to the random distribution of multiple phases over the nano-, micro-, meso- and macro-scales [1-4]. A better understanding of mechanical properties including the failure processes by both experiments and computer modeling has become one of the most critical research topics for concrete [5-7]. Corr *et al.* predicted the mechanical properties of concrete in tension with the consideration of meso-scale randomness in the cohesive interface properties [8]. Cusatis *et al.* formulated the Lattice Discrete Particle Model (LDPM) and simulated experiments include uniaxial and multiaxial compression, tensile fracture, shear strength, and cyclic compression tests [9, 10]. Moreover, concrete was simulated with plasticity-damage constitutive model, and showed a very good correlation with the experimental results [11].

With the emergence of nanoindentation technique, it is available to experimentally measure the properties of the ITZ (Interfacial Transition Zone) between aggregate and mortar matrix [12, 13]. Due to the recent advances in understanding the microstructure, thickness, and mechanical properties of the ITZ and the developments of computational methods, the micromechanical behavior of concrete can be effectively simulated to get a deeper insight into the effect of each phase (such as aggregate size and shape, ITZ thickness and micromechanical properties, and the mortar matrix mechanical properties, etc.).

In this study, Modeled Recycled Aggregate Concrete (MRAC) is a volume element of RAC which is used to simplify the real RAC study. A plastic-damage model is adopted within FEM analysis. The mechanical properties of ITZs in MRAC are obtained by a nanoindentation technique. Two-dimensional microscale numerical modeling is conducted in order to investigate the effects of ITZs on the overall behavior and failure process of MRAC under both uniaxial loadings.

2. Modeled recycled aggregate concrete

The MRAC consists of nine recycled coarse aggregate surrounded by a mortar matrix [5, 14]. Recycled coarse aggregate is idealized to have a round shape. The MRAC used in numerical simulation is shown in Figure 1. The MRAC means the recycled coarse aggregates are embedded within new mortar matrix as a square array. This is an assumption made to simplify the real RAC and provide useful information regarding crack initiation and mechanical response of RAC under loadings. The idealization of regular distribution of recycled coarse aggregates in RAC not only simplifies the problem but also assists in studying the effect of different phases on overall failure behavior of RAC.

(a) MRAC specimen (b) MRAC schematic

Figure 1. Modeled recycled aggregate concrete (MRAC)

3. Constitutive relationships

3.1. Mortar matrix

Mortar matrix shows softening behavior after reaching its peak tensile or compressive stress, which is due to toughening mechanics within the fracture process zone. Both micro-cracking development and irreversible deformations contribute to the nonlinear response of mortar matrix. A plastic-damage constitutive model for mortar matrix is developed by former investigators [11, 15]. Anisotropic damage with a plasticity yield criterion and a damage criterion are introduced to adequately describe the plastic and damaged behavior of mortar matrix.

In order to account for different effects under tensile and compressive loadings, two damage criteria are adopted: one for compression and a second for tension such that the total stress is decomposed into tensile and compressive components. The strain equivalence hypothesis is used in deriving the constitutive equations, so that the strains in the effective (undamaged) and damaged configurations are set equal.

3.2. ITZs

With the emergence of nanoindentation techniques, it is now possible to directly measure the micromechanical properties of the ITZs. A total of 341 indents were performed in an array at each studied area (Figure 3 (a) and (b)). Microhardness testing on cement paste found that there is a linear relationship between microhardness and compressive strength. The hardness obtained from nanoindentation is assumed to provide a linear relationship between

hardness and strength [16, 17]. In this study, the distribution of indentation modulus was used as a basis for the property characteristics of old ITZ and new ITZ, such as the thickness, elastic modulus and strength related to old and new mortar matrix, respectively. Figure 3 (c) and (d) show the indentation modulus distributions with the distance across old ITZ and new ITZ. In this test, greater porosity in the ITZs caused the reduced elastic modulus and strength, relative to those of related mortar matrix.

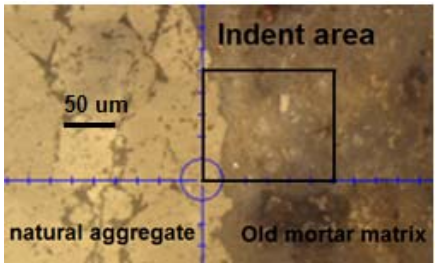

(a) Indent area in old ITZ of RAC

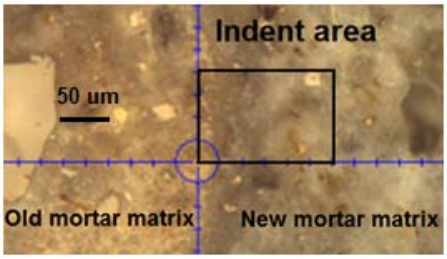

(b) Indent area in new ITZ of RAC

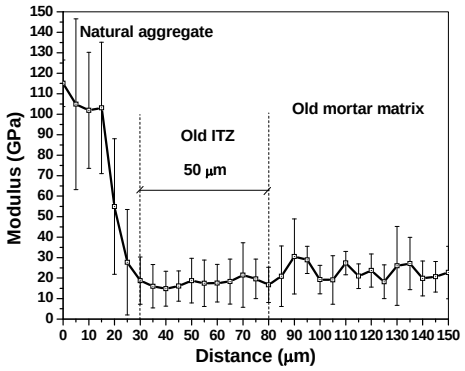

(c) Modulus distribution across old ITZ

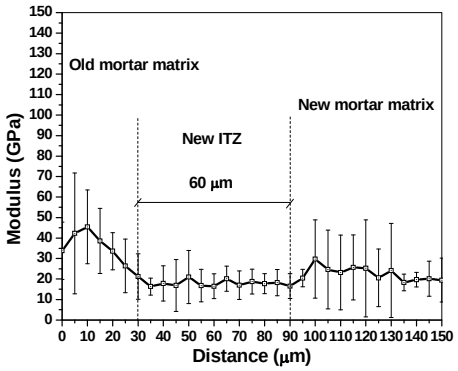

(d) Modulus distribution across new ITZ

Figure 3. Nanomechanical properties of ITZs in RAC [9, 35]

The old ITZ and new ITZ thickness was estimated by locating the places where there is slight variation in the indentation modulus with the distance from the natural aggregate or old mortar matrix surface, and the indentation modulus distribution of the ITZs seem to be close to those of corresponding old mortar matrix and new mortar matrix. Based on the nanoindentation results, the thicknesses of old ITZ and new ITZ are found to be around 50 μm and 60 μm, respectively. Moreover, the average indentation modulus of old ITZ and new ITZ were found to be approximately 80% and 85% of those of old mortar matrix and new mortar matrix, respectively. We choose a linear relationship between indentation hardness and strength. Considering the hardness has a similar distribution with the modulus in the ITZs regions, the strengths of old ITZ and new ITZ are assumed to be 80% and 85% of those of old mortar matrix and new mortar matrix, respectively. For the mortar matrix, elastic modulus, the strength (peak stress), and deformation capacity (peak strain and ultimate strain) parameters are obtained according the experimental data from Refs. [5, 14]. In case of the ITZs, the relative mechanical properties (elastic modulus and strength) to those of mortar matrix can be provided by the nanoindentation test. Combining the descriptions in this and above sections, the predicted uniaxial tensile and compressive stress-strain relationships for both ITZs and mortar matrix based on the plastic-damage constitutive model are shown in Figure. 4.

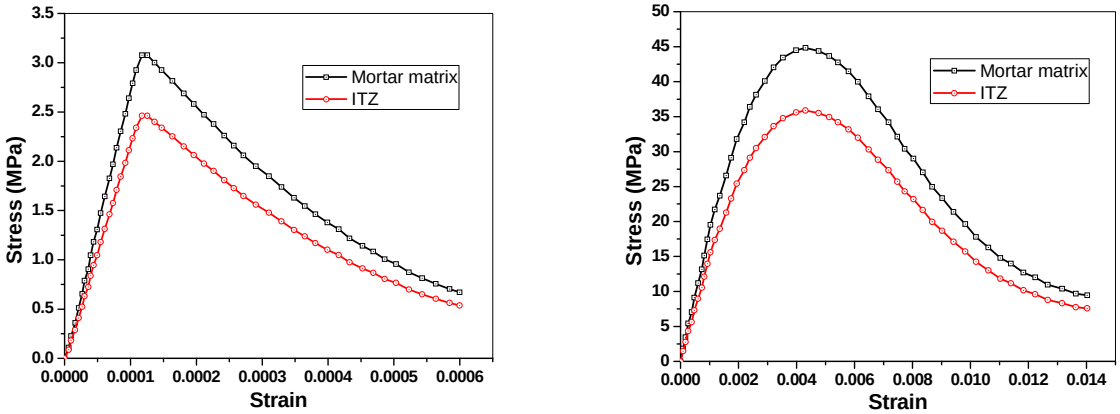

(a) Uniaxial tension (b) Uniaxial compression

Figure 4. Uniaxial stress-strain relation of ITZs and mortar matrix

3.3. Natural aggregate

Granite cylinders are used as natural aggregate in the MRAC. Based on the experiment results [5], there were not cracks or damage observed in the natural aggregates during loading. In the current study, natural aggregate is modeled as linear-isotropic material. It behaves linearly throughout the analysis. For the numerical calibration validation, the materials parameters of each phase in MRAC, which were determined according to the experimental data, are listed in Table 1. However, the Poisson's ratios of new ITZ and old ITZ were defined as 0.20 [18].

Table 1. Material properties of each phase in MRAC

MRAC	Thickness (μm)	Elastic modulus (GPa)	Poisson's ratio (ν)	Strength (MPa)	
				Compressive (f_c)	Tensile (f_t)
Natural aggregate	—	80.0	0.16	—	—
Old mortar (OM)	—	25.0	0.22	45.0	3.00
New mortar (NM)	—	23.0	0.22	41.4	2.76
Old ITZ (OI)	50.0	20.0	0.20	36.0	2.40
New ITZ (NI)	60.0	18.0	0.20	33.1	2.21

4. FEM simulation and test verification

4.1. FEM model

The software program (ABAQUS 6.11) was used for the FEM analyses. 4-node plane stress quadrilateral (CPS4R) elements were used to mesh the MRAC. The 2D micro-scale FEM model of MRAC is shown in Figure 5. The model was subjected to a uniformly distributed displacement at the top edge, as the displacement-controlled loading scheme was used. The *Y* degrees of freedom were fixed at the bottom edge, while the *X* degrees of freedom and rotation were not constrained. The FEM model has a total of 34240 elements in this simulation.

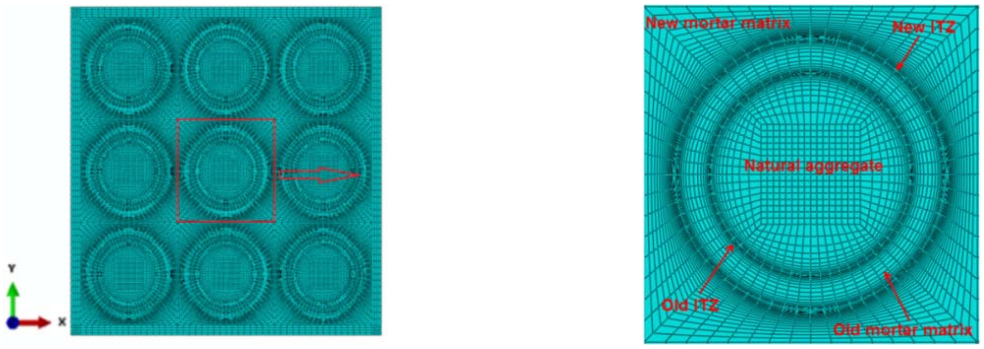

(a) Overall FEM model (b) Details of each phase

Figure 5. 2D micro-scale FEM model of MRAC

4.2. Modeling implementation

In this paper, ABAQUS/explicit quasi-static analyses were applied for the numerical simulation [19, 20, 21]. The ABAQUS/explicit quasi-static solver used an analysis time of 0.1 second (period time). A displacement-controlled loading scheme was adopted in this simulation. In order to obtain complete stress-strain curves, after trial and comparison, all the analyses for uniaxial tension and compression were ended at a displacement d=0.09 mm (ultimate strain 0.0006) and 0.9 mm (ultimate strain 0.006), respectively.

The FEM numerical response depends on two sets of parameters. The first set is relevant to the tensile and compressive stress data which are provided as a tabular function of strain, which is directly obtained from the constitutive relation of each phase in MRAC. These mechanical properties are provided by experimental study and mix design. The other one is the definition of the damage variable as a tabular function of the inelastic strain for both the tensile and compression. If the damage variable is specified, ABAQUS automatically calculates the inelastic and plastic strain values.

Generally, the maximum tensile stress (S_{11}) tends to concentrate mainly in the ITZs in Figure 6. These stress concentrations could lead to the development of microcracks along these regions, which in turn could lead to the failure of the MRAC. As the properties of the ITZs are weaker than those of other phases in the MRAC, the stress concentrations mainly occur in these regions and may lead to or promote the failure. Experimental results also proved that bond cracks firstly appeared around the weak ITZs, and then propagated into the mortar by connecting with each other [5, 14].

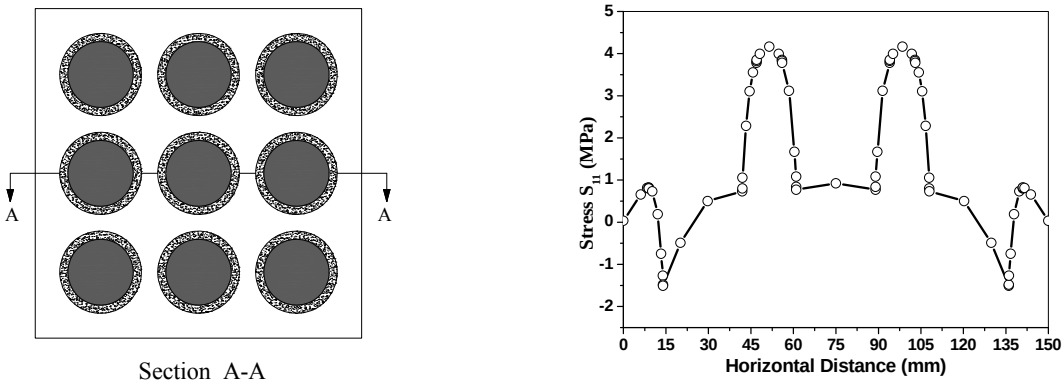

Section A-A

(a) Cross section in MRAC (b) Tensile stress S_{11} distribution

Figure 6. Stress distribution for section A-A

4.3. Simulation results

4.3.1. Uniaxial compression

According to the above parameters and descriptions, the complete compressive stress-strain curve and failure process of MRAC under uniaxial compression loading were calculated. In order to calibrate and validate the FEM, the MRAC was studied by compression test using Digital Image Correlation (DIC) technique [5, 14]. The experimental data are relevant to compression tests on MRAC specimens with the same old cement mortar mixture design (w/c=0.45) but three different new cement mortar mixture designs (w/c=0.36, 0.45, and 0.55). The mixture proportion details of MRAC specimens are listed in Table 2. The experimental setup and basic failure pattern are shown in Figure 7.

Table 2. Mixture proportion of cement mortar in MRAC [5]

MRAC	Old mortar (w/c ratio)	Mass, kg/m^3			New mortar (w/c ratio)	Mass, kg/m^3		
		Water	Cement	Sand		Water	Cement	Sand
MRAC-30-20	0.45	160	356	565	0.55	160	276	589
MRAC-30-30	0.45	160	356	565	0.45	160	356	565
MARC-30-40	0.45	160	356	565	0.36	160	444	539

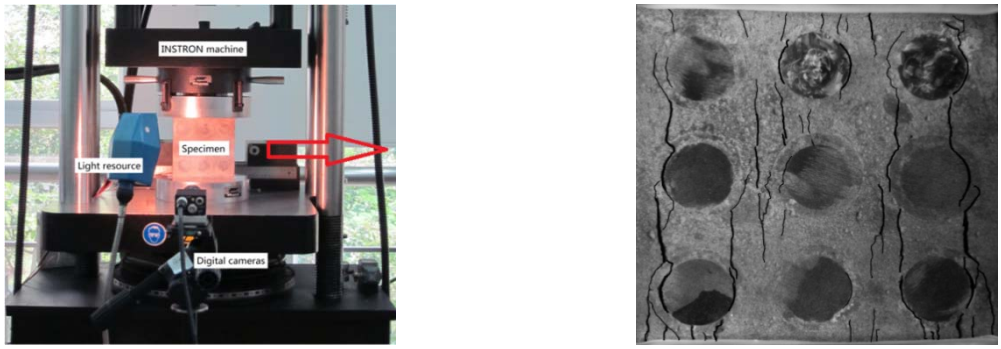

(a) Experimental and DIC setup (b) MRAC failure pattern

Figure 7. Experimental study on MRAC under uniaxial compression [5, 14]

To investigate the compressive stress-strain curve and crack propagation of MRAC, numerical simulation relevant to the mechanical behavior of MRAC with different new mortar matrix and corresponding new ITZ under uniaxial loading is considered herein. The analysis was conducted on MRAC specimens with one mixture for old cement mortar and three mixtures for new cement mortar (MRAC30-20, MRAC30-30 and MRAC30-40). For the real MRAC, the properties of old/new ITZ properties are actually somewhat related or proportional to the old/new mortar matrix properties. When varying the relative mechanical properties of new mortar matrix to old mortar matrix, the relative mechanical properties between new ITZ and new mortar matrix were kept constant with a ratio of 0.85. The different stress-strain curves of MRAC are shown and compared in Figure 8. It is also found that the peak stress and strain increase with the decrease of water-to-cement ratio of the new mortar matrix.

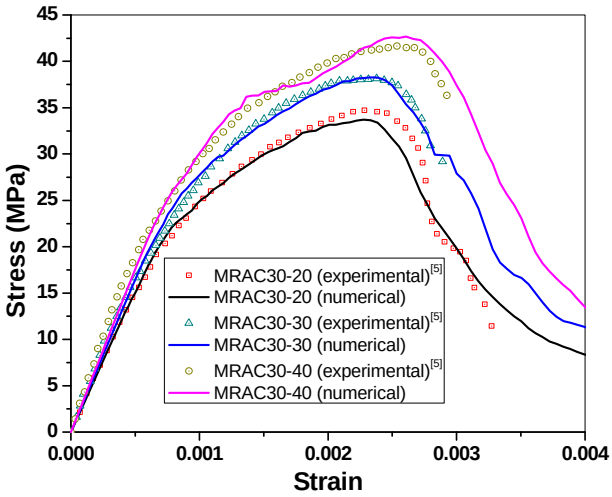

Figure 8. Compressive stress-strain curves of MRAC

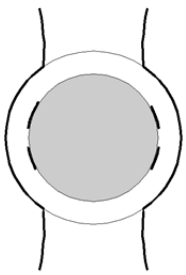

(a) MRAC30-20 (Experimental) [5]

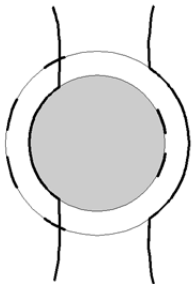

(b) MRAC30-30 (Experimental) [5]

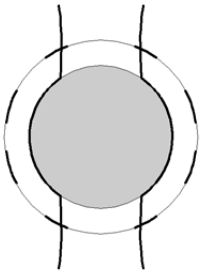

(c) MRAC30-40 (Experimental) [5]

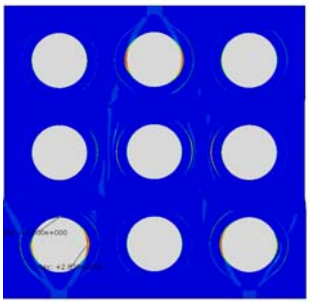

(d) MRAC30-20 (Numerical)

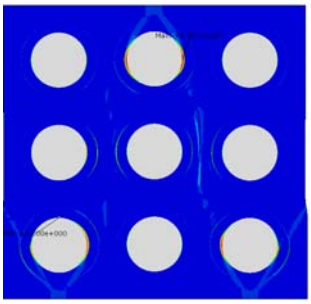

(e) MRAC30-30 (Numerical)

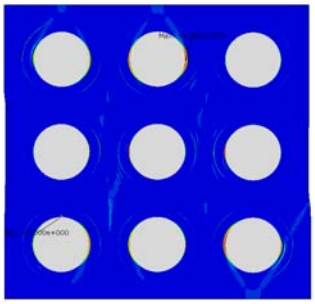

(f) MRAC30-40 (Numerical)

Figure 9. Simulated microcrack development under compression

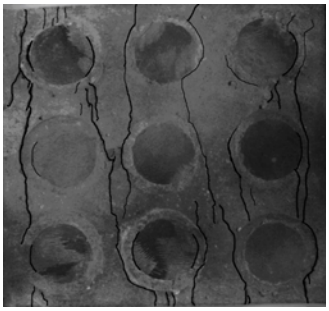

(a) MRAC30-20 (Experimental) [5]

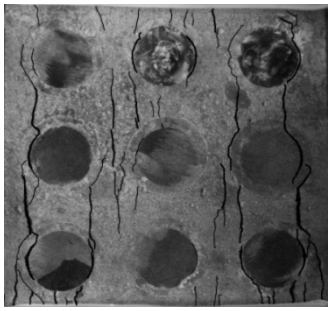

(b) MRAC30-30 (Experimental) [5]

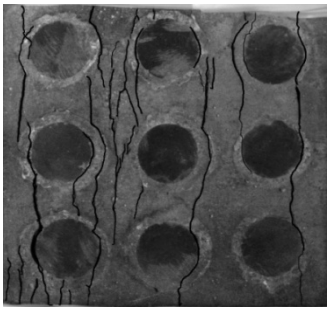

(c) MRAC30-40 (Experimental)[5]

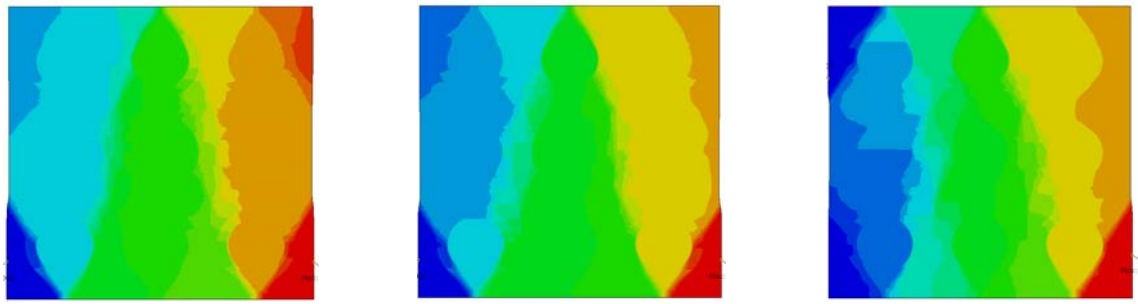

(d) MRAC30-20 (Numerical) (e) MRAC30-30 (Numerical) (f) MRAC30-40 (Numerical)

Figure 10. Simulated failure pattern of MRAC under compression

From Figure 9, it can be revealed that the micro-crack formations are quite different for the different MRAC specimens, which fits the experimental results very well [10, 49]. In the case of MRAC30-20, most of the first observable micro-cracks appeared at the new ITZ in quantity. As for the MRAC30-30, the first observable micro-cracks formed around both old and new ITZ. In the MRAC30-40, most of the first observable micro-cracks initiated at the old ITZ. With the comparison between experimental and numerical micro-cracks initiation, it can be concluded that the numerical results agree well with the experimental evidences. Figure 10 represents the numerical failure pattern for MRAC under uniaxial compression. With the load increasing, micro-cracks, which were found around the ITZs, start connecting with each other, and cross the old mortar matrix regions. Finally, the cracks propagate into new mortar parallel to the loading direction. From the view point of failure pattern of MRAC, the numerical results are also in good agreement with the experimental ones [5, 14].

4.3.2 Uniaxial tension

The numerical tensile stress-strain curves of MRAC with different new mortar matrix are presented in Figure 11. It appears that both the pre-peak load and post-peak load behavior are influenced by the mechanical properties of new mortar matrix. It can be clearly seen that the pre-peak region is nearly linear, while in the post-peak load region there is a subsequently steep drop of load and a long tail. The jumps in the post-peak load stage are due to the crack opening. The tensile strength and elastic modulus of MRAC increase with the increase of the mechanical properties of new mortar matrix. However, the model with higher mechanical properties exhibits less ductility than that with lower mechanical properties of new mortar matrix. This numerical evidence shows a good agreement with the experimental tendency of normal concrete model [8]. For the stress-strain curves, the crack localization corresponds to the steep branch after the peak stress, and mortar matrix prevails on the ITZs failure in the tail of the softening curves. However, ITZs failure still exists in the post-peak stage such as the slipping effect.

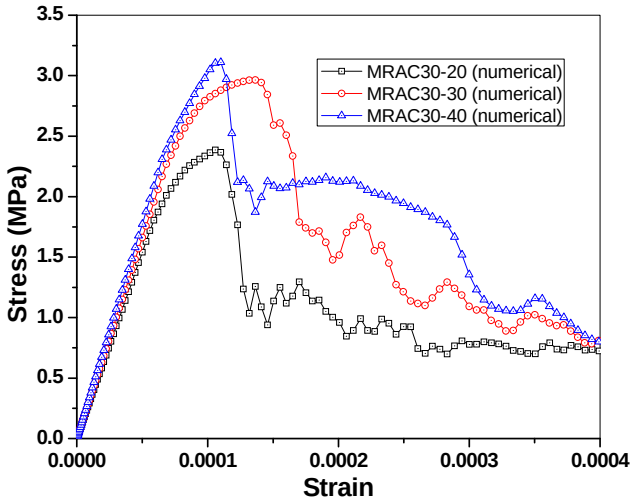

Figure 11. Tensile stress-strain curve of MRAC

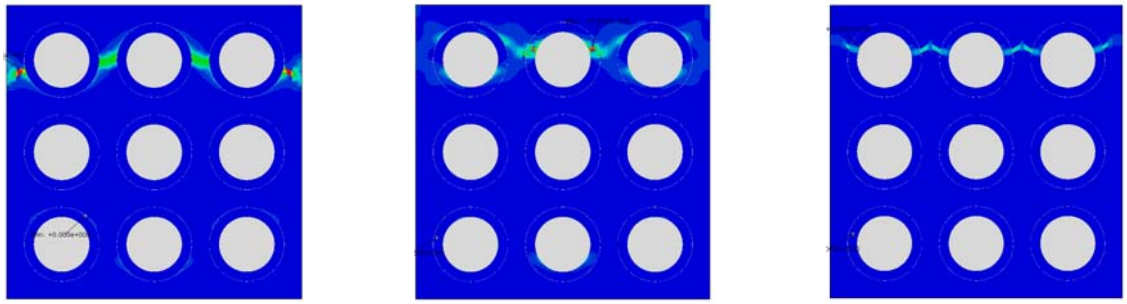

(a) MRAC30-20 (b) MRAC30-30 (c) MRAC30-40

Figure 12. Simulated microcrack development under tension

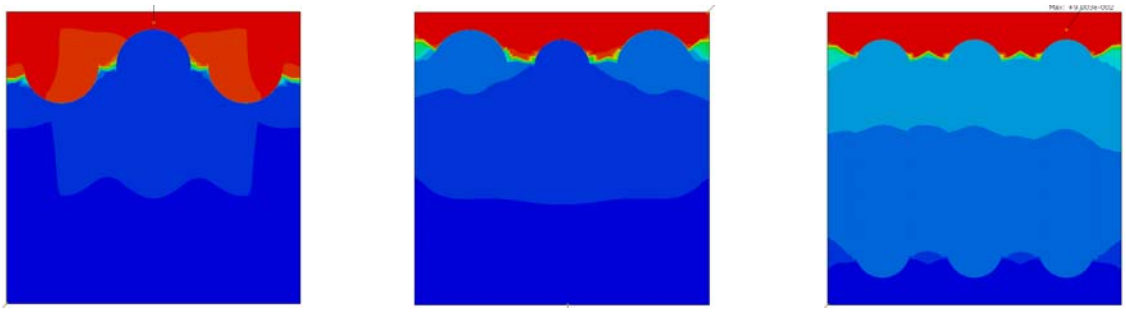

(a) MRAC30-20 (b) MRAC30-30 (c) MRAC30-40

Figure 13. Simulated failure pattern of MRAC under tension

The micro-crack propagation for the MRAC models at the peak loading level is shown Figure 12. It can be seen that strain concentrations are clear around the ITZs. It can be found that the failure cracks initiate in ITZs, and propagate laterally until the whole failure. These results show that the different new mortar matrix produces a different ITZ failure. In the case of MRAC30-20, micro-crack localization occurs around the new ITZ. For MRAC30-30, the micro-crack concentration formed at both new ITZ and old ITZ. However, for MRAC30-40, the localization process mainly forms at the old ITZ. The similar cracking localization is also observed in MRAC under compression in the experimental research [5,14]. This phenomenon is due to the competition between micro-cracks located at old ITZ and new ITZ. Moreover, the final configuration is dependent on the relative strength of new mortar matrix to old mortar matrix.

Figure 13 shows vertical displacement contour maps of MRAC at post-peak load stage. At the post-peak loading stage, with the load increasing, macro-cracks propagate across the old mortar matrix, and start to develop in both ITZs and mortar matrix regions. For MRAC30-20, the main failure macro-crack forms around the new ITZ and propagates through the new mortar matrix laterally until the whole failure. While for MRAC30-30, the main failure crack develops around both new ITZ and old ITZ, and propagates through both old and new mortar matrix. However, for the MRAC30-40, the main failure crack goes around the old ITZ and propagates across the old and new mortar matrix.

5. Conclusions

Numerical simulations of Modeled Recycled Aggregate Concrete (MRAC) under both uniaxial compression and uniaxial tension loadings have been presented. The effects of properties of new mortar matrix and ITZs on the stress-strain response and fracture process are investigated. The main conclusions can be drawn as follows:

(1) The constitutive relation of the ITZ is proposed within the framework of a plastic-damage plasticity constitutive model. The constitutive relation is similar to that of the mortar matrix, but the elastic modulus and strength are lower than those of the mortar matrix;
(2) The FEM modeling is capable of simulating the complete stress-strain curve, as well as the overall fracture patterns including localization of deformation and the micro-crack pattern. Fine agreement between experimental and numerical results is obtained in the calibration and validation;
(3) The new mortar matrix and new ITZ has a significant influence on the stress-strain responses and failure patterns of MRAC. With the increase in the mechanical properties of the new mortar matrix, the strength increases correspondingly, and the micro-crack localization mitigates from the new ITZ to the old ITZ;
(4) It can be concluded that the mechanical damage plasticity model simulations provide valuable insights into the relationship between nano/micro-scale mechanical properties and macro-scale mechanical behavior in recycled aggregate concrete.

Acknowledgements

The authors would like to acknowledge the financial support from the National Natural Science Foundation of China (51178340). The authors gratefully acknowledge Prof. John Bolander in University of California, Davis for his constructive comments and suggestions. The first author would also like to thank China Scholarship Council (CSC) for its financial support during his study at Northwestern University.

References

[1] N. Tregger, D. Corr, L. Graham-Brady, S. Shah, Modeling the effect of mesoscale randomness on concrete fracture. Probabilistic Engineering Mechanics, 21(2006) 217-225.
[2] W.G. Li, J.Z. Xiao, Z.H. Sun, S. Kawashima, S.P. Shah, Interfacial transition zones in recycled aggregate concrete with different mixing approaches. Construction and Building Materials, 35(2012) 1045-1055.
[3] M. Yip, Z. Li, B.S. Liao, J.E. Bolander, Irregular lattice models of fracture of multiphase particulate materials. International Journal of Fracture, 140(2006) 113-124.
[4] G. Lilliu, J.G.M. van Mier, On the relative use of micro-mechanical lattice analysis of 3-phase particle composites. Engineering Fracture Mechanics, 74(2007) 1174-1189.
[5] J.Z. Xiao, W.G. Li, Z.H. Sun, S.P. Shah, Crack propagation in recycled aggregate concrete under uniaxial compressive loading. ACI Materials Journal, 109(2012)

451-461.
[6] J.Z. Xiao, W.G. Li, D.J. Corr, S.P. Shah, Simulation study on the stress distribution in modeled recycled aggregate concrete under uniaxial compression. Journal of Materials in Civil Engineering, in press, 2012.
[7] D. Asahina, E.N. Landis, J.E. Bolander, Modeling of phase interfaces during pre-critical crack growth in concrete. Cement and Concrete Composites, 33(2011) 966-977.
[8] D. Corr, M. Accardi, L. Graham-Brady, S. Shah, Digital image correlation analysis of interfacial debonding properties and fracture behavior in concrete. Engineering Fracture Mechanics, 74 (2007) 109-121.
[9] G. Cusatis, D. Pelessone, A. Mencarelli, Lattice Discrete Particle Model (LDPM) for concrete failure behavior of concrete. I: Theory. Cement and Concrete Composites, 33(2011) 881-890.
[10] G. Cusatis, A. Mencarelli, D. Pelessone, Baylot J, Lattice Discrete Particle Model (LDPM) for failure behavior of concrete. II: Calibration and Validation. Cement and Concrete Composites, 33(2011) 891-905.
[11] S.M. Kim, R.K. Abu Al-Rub, Meso-scale computational modeling of the plastic-damage response of cementitious composites. Cement and Concrete Research, 41(2011) 339-358.
[12] P. Mondal, S.P. Shah, L.D. Marks, Nanoscale characterization of cementitious materials. ACI Materials Journal, 105(2008) 174-179.
[13] J.Z. Xiao, W.G. Li, Z.H. Sun, D.A. Lange, S.P. Shah, Studying interfacial transition zones in recycled aggregate concrete with nanoindentation. Cement & Concrete Composite, in press, 2012.
[14] W.G. Li, J.Z. Xiao, Z.H. Sun, P. S.P. Shah, Failure processes of modeled recycled aggregate concrete under uniaxial compression. Cement & Concrete Composites, 34 (2012)1149-1158.
[15] U. Cicekli, G.Z. Voyiadjis, R.K. Abu Al-Rub, A plasticity and anisotropic damage model for plain concrete. International Journal of Plasticity, 23(2007)1874-1900.
[16] S. Igarashi, A. Bentur, S. Mindess, Microhardness testing of cementitious materials. Advanced Cement Based Materials, 4(1996) 48-57.
[17] C. Bobko, F.-J. Ulm, The nano-mechanical morphology of shale. Mechanics of Materials, 40 (2008) 318-337.
[18] G. Ramesh, E.D. Sotelino, W.F. Chen, Effect of transition zone on elastic moduli of concrete materials. Cement and Concrete Research, 26(1996) 611-622.
[19] Z.J. Yang, X.T. Su, J.F. Chen, G.H. Liu, Monte Carlo simulation of complex cohesive fracture in random heterogeneous quasi-brittle materials. International Journal of Solids and Structures, 46 (2009) 3222-3234.
[20] H.X. Yu, I.W. Burgess, J.B. Davison, R.J. Plank, Numerical simulation of bolted steel connections in fire using explicit dynamic analysis. Journal of Constructional Steel Research, 64(2008) 515-525.
[21] Version 6.11 Theory Manual, ABAQUS, 2011.